Yong Teng
Department of Physiology and Biomedical Engineering, Mayo Clinic College of Medicine, Rochester, MN 55905;
Department of Orthopedic Surgery, Mayo Clinic College of Medicine, Rochester, MN 55905;
Orthopedic Center, General Hospital of Xinjiang Military Region PLA, Uygur Autonomous Region, Xinjiang 830000, China
e-mail: orthtengyong@163.com

Hugo Giambini
Department of Orthopedic Surgery, Mayo Clinic College of Medicine, Rochester, MN 55905
e-mail: giambini.hugo@mayo.edu

Asghar Rezaei
Department of Physiology and Biomedical Engineering, Mayo Clinic College of Medicine, Rochester, MN 55905
e-mail: rezaei.asghar@mayo.edu

Xifeng Liu
Department of Physiology and Biomedical Engineering, Mayo Clinic College of Medicine, Rochester, MN 55905;
Department of Orthopedic Surgery, Mayo Clinic College of Medicine, Rochester, MN 55905
e-mail: liu.xifeng@mayo.edu

A. Lee Miller, II
Department of Orthopedic Surgery, Mayo Clinic College of Medicine, Rochester, MN 55905
e-mail: miller.alan@mayo.edu

Brian E. Waletzki
Department of Orthopedic Surgery, Mayo Clinic College of Medicine, Rochester, MN 55905
e-mail: waletzki.brian@mayo.edu

Lichun Lu[1]
Department of Physiology and Biomedical Engineering, Mayo Clinic College of Medicine, Rochester, MN 55905;
Department of Orthopedic Surgery, Mayo Clinic College of Medicine, Rochester, MN 55905
e-mail: lu.lichun@mayo.edu

Poly(Propylene Fumarate)–Hydroxyapatite Nanocomposite Can Be a Suitable Candidate for Cervical Cages

A wide range of materials have been used for the development of intervertebral cages. Poly(propylene fumarate) (PPF) has been shown to be an excellent biomaterial with characteristics similar to trabecular bone. Hydroxyapatite (HA) has been shown to enhance biocompatibility and mechanical properties of PPF. The purpose of this study was to characterize the effect of PPF augmented with HA (PPF:HA) and evaluate the feasibility of this material for the development of cervical cages. PPF was synthesized and combined with HA at PPF:HA wt:wt ratios of 100:0, 80:20, 70:30, and 60:40. Molds were fabricated for testing PPF:HA bulk materials in compression, bending, tension, and hardness according to ASTM standards, and also for cage preparation. The cages were fabricated with and without holes and with porosity created by salt leaching. The samples as well as the cages were mechanically tested using a materials testing frame. All elastic moduli as well as the hardness increased significantly by adding HA to PPF ($p < 0.0001$). The 20 wt % HA increased the moduli significantly compared to pure PPF ($p < 0.0001$). Compressive stiffness of all cages also increased with the addition of HA. HA increased the failure load of the porous cages significantly ($p = 0.0018$) compared with nonporous cages. PPF:HA wt:wt ratio of 80:20 proved to be significantly stiffer and stronger than pure PPF. The current results suggest that this polymeric composite can be a suitable candidate material for intervertebral body cages. [DOI: 10.1115/1.4040458]

[1]Corresponding author.
Manuscript received January 19, 2018; final manuscript received May 29, 2018; published online June 21, 2018. Assoc. Editor: James C. Iatridis.

Introduction

Bone and joint degenerative diseases affect more than 1.7 billion people worldwide [1]. Such diseases lead to the degradation of the bones in the spine, hip, and knee due to abnormal bone tissue and large loading or lack of the normal biological self-healing process [2]. Biomaterials are natural or artificial materials used for implant design to replace lost or injured biological tissues. Biomaterials are used in many different areas of health care, and the numbers of implants used in spine, knee, and hip are extremely high and continue to increase due to advancements in the field [2].

Cage devices have been used for interbody spine fusion to enhance the stability of the spine and prevent postoperative collapse of the vertebral bodies [3]. Metals, composites, ceramics, and polymers have been previously implemented to develop spinal cages and stabilize the spine while also promoting bony ingrowth [4]. Early metallic devices, still used in clinical practice, were developed to achieve suitable physical properties with minimal toxic effects. However, these metallic implants are substantially stiffer than bone, increasing the motion stiffness of the spine segments [5] and causing migration of the gage or pseudarthrosis [6]. Other materials, such as carbon fiber, have also been used to develop cages. However, although these cages present similar stiffness to the surrounding bone tissue, decreasing the likelihood of stress shielding, carbon fiber cannot be chemically bonded to grafted bone tissues [7].

Advancements in the tissue engineering field have contributed to the development of promising materials to provide attractive alternatives for spine fusion and intervertebral cages. Poly(propylene fumarate) (PPF) is one of these attractive polymers with many potential applications in orthopedics [8]. PPF is biodegradable, biocompatible and has been shown to be a good replacement for trabecular bone tissue [9]. However, PPF is not able to provide material properties to closely match those of cortical bone. Hydroxyapatite (HA) is a bioceramic with chemical composition and morphology similar to that of bone. In addition to being biocompatible and provide good osteoconductivity [10,11] HA presents much higher mechanical properties when compared to PPF.

The goal of this study, therefore, was to assess the effect of various formulations of PPF–HA composites on mechanical properties in the setting of intervertebral cages. The aims of the study were twofold: first, to characterize thermal and material properties using ASTM standards of various bulk PPF–HA formulations (PPF:HA, wt:wt ratios of 100:0, 80:20, 70:30, and 60:40); and second, to fabricate and evaluate the mechanical properties of intervertebral cages using the above mentioned formulations.

Materials and Methods

Poly(propylene fumarate)–hydroxyapatite composites were fabricated and mechanically tested as bulk material and as a finished product in the shape of intervertebral body cages. Figure 1 shows a flowchart illustrating the bulk material and cage development and characterization. All materials used in this study were obtained from Sigma–Aldrich (Milwaukee, WI) unless noted otherwise.

Synthesis of Polypropylene Fumarate. Poly(propylene fumarate) was synthesized as previously described [12]. Briefly, diethyl fumarate (DEF) and 1,2-propylene glycol were mixed together at a molar ratio of 1:3. Hydroquinone and zinc chloride were added to diethyl fumarate as a polymerization inhibitor and as a catalyst, respectively, in a 0.002:0.01:1 molar ratio. Fumaric diester was obtained by transesterification by heating the solution at 100 °C for 1 h and then at 150 °C for 7 h. The solution was allowed to cool to 100 °C and then placed under vacuum (<1 mmHg). The polymerization reaction was then run at 150 °C for 5 h. Before storing the PPF, gel permeation chromatography was performed to evaluate its molecular weight.

Fabrication of Poly(Propylene Fumarate):Hydroxyapatite Composites. Hydroxyapatite pellet nanoparticles (diameters ranging 20–100 nm) were purchased from Berkeley Advanced Biomaterials (Berkeley, CA). PPF:HA nanocomposite scaffolds were prepared using a previously established method [13]. Briefly,

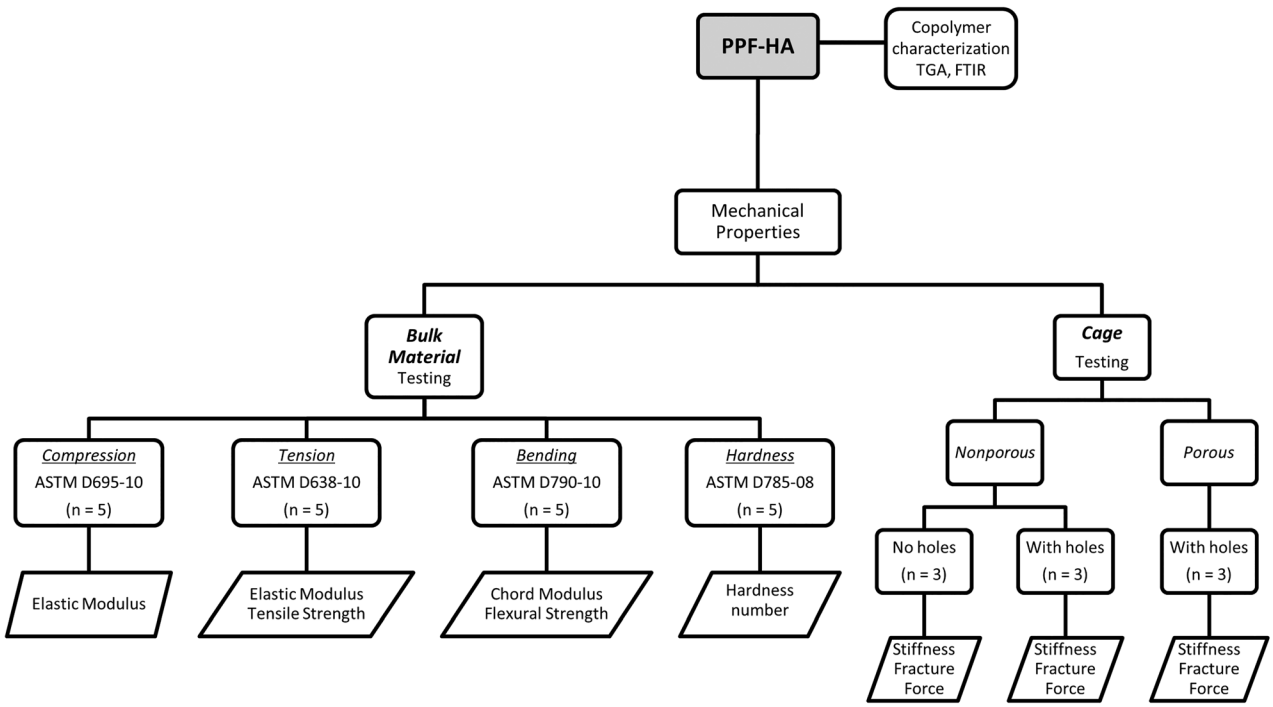

Fig. 1 Flowchart describing the bulk material and cage characterization. This sequence of testing events was followed for each polymer group (PPF; PPF:HA (80:20); PPF:HA (70:30); and PPF:HA (60:40)). Bulk material was characterized by TGA and FTIR, and by ASTM standards for compression, tension, bending, and hardness. Nonporous (with/without holes) and porous (with holes) cages were tested in compression.

35.48 g of PPF was mixed in 11.83 g of DEF with a PPF:DEF wt:wt ratio of 75:25 and placed in a 80 °C oven overnight to completely dissolve the PPF. After cooling to room temperature, 1.5 wt % of photoinitiator bis(2,4,6-trimethylbenzoyl) phenylphosphine oxide (BAPO) was added to the PPF:DEF mixture and placed on a shaker for 24 h (protected from light) to obtain a homogenous PPF/DEF/BAPO solution. To fabricate PPF:HA nanocomposites with PPF:HA wt/wt ratios of 100:0, 80:20, 70:30, and 60:40, the corresponding amounts of nano-HA particles were added to the PPF/DEF/BAPO solution and allowed to mix completely for 24 h under shaking (protected from light). The homogeneous PPF/DEF/BAPO/HA mixture was then transferred into various glass molds and placed under UV light with a distance of approximately 7 cm from the lamp head for 30 min to allow for crosslinking. Finally, the crosslinked PPF:HA was then removed from the molds after being cooled down to ambient temperature. The four polymer groups consisted of the following wt:wt combination of PPF and HA: PPF; PPF:HA (80:20); PPF:HA (70:30); PPF:HA (60:40).

Cage Design and Fabrication

Nonporous Cages. Clear plexiglass sheets were obtained for fabrication of the mold. The mold consisted of two upper and lower parts with outer dimensions of 2 in × 2 in. In the center of the plexiglass mold, a hollow cavity, with the shape of an intervertebral cage was fabricated. PPF:HA, in its various formulations, was injected into the mold to create the cages. Two groups of cages were developed: *No holes* (cages containing no holes on the surface); *holes*: cages containing small drilled holes around the cages to potentially allow for future bone ingrowth. Twelve cages with and without holes were fabricated for a total of 24 samples (three cages per polymer configuration).

Porous Cages. In order to potentially allow for additional bone ingrowth, porous cages were fabricated using NaCl particles of 106–300 μm. NaCl particles were added to the homogeneous PPF/DEF/BAPO/HA mixture at 50 wt %. The mixture was allowed to photocrosslink in the cage mold. Following removal from the mold, the crosslinked cage was placed in a large glass beaker filled with ddH_2O to leach out the salt particles. A magnetic stir bar was used to stir the solution at 200 rpm for 24 h. Frequent water changes (>10 times) were performed to facilitate salt leaching. In total, 12 porous cages (three for each polymer configuration) with drilled holes were fabricated.

Copolymer Characterization

Thermogravimetric Analysis (TGA). TGA was performed for each polymer group/batch using a Discovery TGA (TA instrument, New Castle, DE) at a heating rate of 10 °C min^{-1} from ambient temperature up to 700 °C. Thermograms were used to determine composition-dependent onset of degradation temperature and residual HA in correlation with precursor PPF:HA ratio.

Fourier Transform Infrared Spectroscopy. To explore the composition variance, all composite materials were characterized by attenuated total reflectance Fourier transform infrared spectroscopy (ATR-FTIR) spectra using a Nicolet Continuum Infrared Microscope (Thermo Scientific, Waltham, MA). Briefly, the pure PPF materials, series of PPF–HA nanocomposite materials (PPF:HA, wt:wt ratios of 80:20, 70:30, and 60:40), as well as the pure HA components, were compressed to dense pellets with exclusion of air bubbles. Before the test, a homogeneous flat surface was determined under microscope, and the FTIR probe was located gently onto the surface with direct contact. A spectrum was obtained with wavenumbers set from 650 to 4000 cm^{-1} and resolution at 4 cm^{-1}. For each polymer group, four samples were tested and a typical spectrum was selected and compared.

Mechanical Properties. Mechanical properties of the four polymer groups (PPF; PPF:HA (80:20); PPF:HA (70:30); PPF:HA (60:40)) were obtained using a Mini Bionix 858 servohydraulic test machine (MTS, Eden Prairie, MN; 16 kN capacity load cell) and based on ASTM International Standards (*compression*: D695-10; *tension*: D638-10; *bending*: D790-10; *hardness*: D785-08). Figure 1 shows the testing setup for mechanical testing of the materials under compression, tension, and bending.

Compression. For each PPF–HA polymer group configuration, five standard cylindrical samples of 6 mm in diameter and 24 mm in length were prepared to reach an approximate slenderness ratio of 11. The cylinders were tested at room temperature under compression at a rate of 1.3 mm/min. Force versus displacement data were recorded and stress versus strain curves were obtained from the acquired data and initial dimensions of the cylinders. Modulus of elasticity was calculated from the linear portion of the curve. Figure 2(*a*) shows a sample undergoing compression testing.

Cages (nonporous/porous and with/without holes) fabricated with the various polymer configurations were also tested in compression to obtain their mechanical properties.

Tension. Five standard type IV dumbbell-shaped samples were prepared from each polymer group using a mold. Sample dimensions were approximately as follows: overall length 115 mm, length at the narrow section 33 mm, gage length 25 mm, and thickness 3.2 mm. Samples were placed on the MTS fixture with the long axis of the samples and the grips aligned with the axis of loading. An extensometer was implemented to measure intrinsic displacement of the material. The samples were loaded to failure at room temperature, and stress versus strain curves were calculated from the force/displacement outcomes and specimen dimensions. Tensile strength and elastic modulus were then calculated. Figure 2(*b*) shows a sample undergoing tensile testing.

Bending. Five flat rectangular bars of length, width and thickness of 80 mm, 12.7 mm, and 2.5 mm, respectively, were prepared from each group. The samples were rested on two supports and loaded at room temperature to determine flexural properties. The span between the two supports was set to 40 mm. Figure 2(*c*) shows the testing setup. The support span was determined, and the specimens were deflected until rupture occurred in the outer surface. Force versus displacement data were collected and flexural stress and strain were subsequently plotted to determine the strength and modulus. Maximum flexural strength, determined as the maximum stress, was calculated as follows:

$$\sigma = \frac{3PL}{2bd^2}$$

where P is the load at a given point on the force/displacement curve (N), L is the support span (mm), b is the width of beam tested (mm), and d is the depth of beam tested (mm).

Modulus was calculated from the linear region of the stress versus strain curve.

Hardness. The Rockwell hardness test (Rockwell Hardness scale "M") was used to determine the indentation hardness of the various polymer groups. A Rockwell hardness number represents the net increase in indented depth as the load on an indenter increases from a fixed small load (10 kg) to a large load (100 kg) and then returned to the minor load. The tested polymer groups consisted of square samples with a length and thickness of 25 mm and 6 mm, respectively. The indenter consisted of a round steel ball of 6.35 mm in diameter. Five indents were performed in each sample to obtain a mean (SD). The Rockwell hardness numbers are presented with the scale symbol representing the indenter size, load, and dial scale used.

Statistical Analysis. JMP version 10.0.0 (SAS Institute, Inc., Cary, NC) was used for statistical analysis. In all analyses, the outcomes were the measured moduli, strength, stiffness, and/or failure load. Analysis of variance (ANOVA) was used to compare different material configurations and the significance of HA.

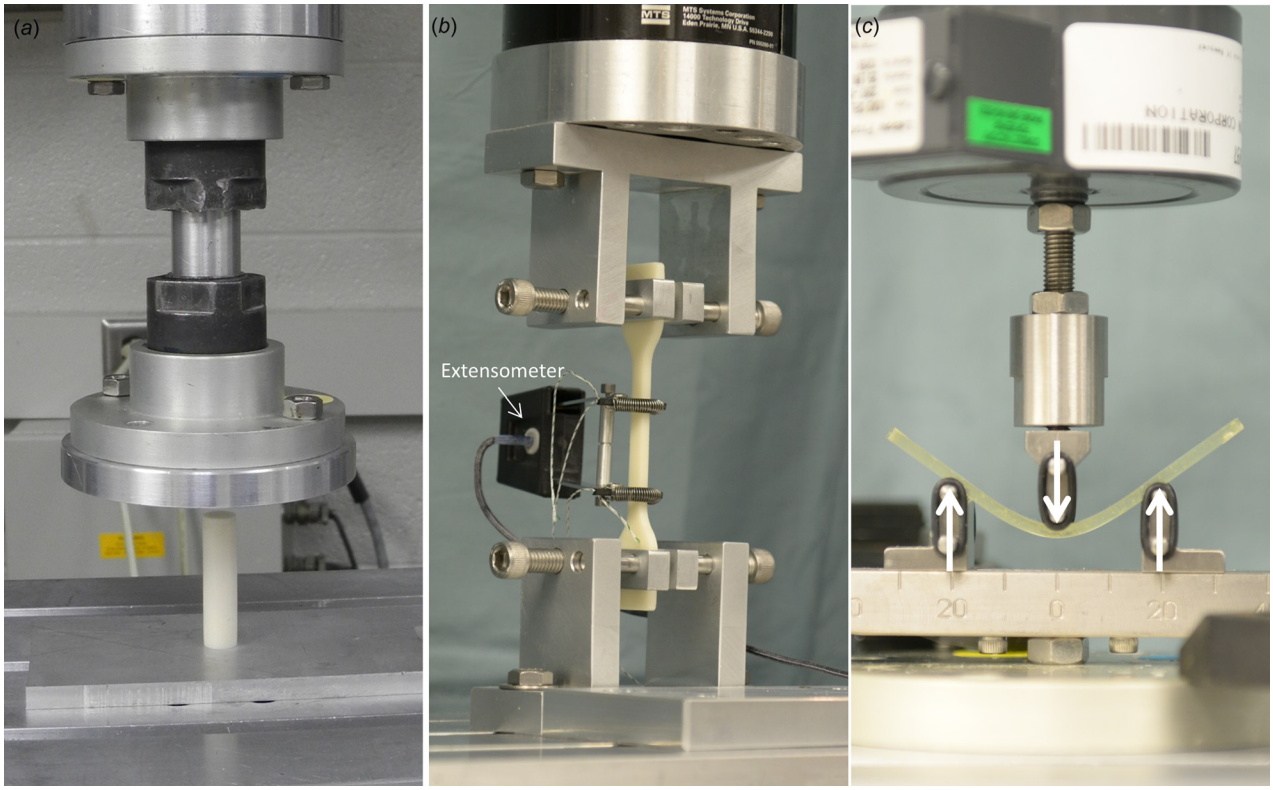

Fig. 2 Mechanical testing setup for (*a*) compression (cylindrical samples of 6 mm in diameter and 24 mm in length), (*b*) tension (standard type IV dumbbell-shaped samples with an overall length 115 mm, length at the narrow section 33 mm, and thickness 3.2 mm), and (*c*) three-point bending (rectangular bars of length, width and thickness of 80 mm in length

ANOVA was also used to compare the cages with the four polymer configurations ($n = 9$ in each polymer configuration), and differences in stiffness among cages with holes ($n = 12$), cages with no holes ($n = 12$), and cages with holes and porosity ($n = 12$). Data are shown using scatter plots with median as previously described [14]. The level of significance was set to 0.05.

Results

Poly(propylene fumarate) with a molecular weight of 2000 g/mol, as measured by gel permeation chromatography, was successfully synthesized. Figure 3(*a*) shows the thermal degradation of the PPF:HA polymer groups. The onset of degradation was similar for all polymer groups, at about 375 °C. The maximum weight loss of more than 90% was found to be for pure PPF. The weight loss for the other groups were about 75%, 65%, and 55% for the PPF:HA (80:20), PPF:HA (70:30), and PPF:HA (60:40), respectively. Figure 3(*b*) shows the FTIR spectra results from the various groups. As illustrated, a new peak arises at about 1000 cm^{-1} that is characteristic of phosphate groups in HA.

Bulk Material Properties

Elastic Moduli. Fig. 4 shows the elastic moduli for each material group in compression, tension, and bending. The mean elastic

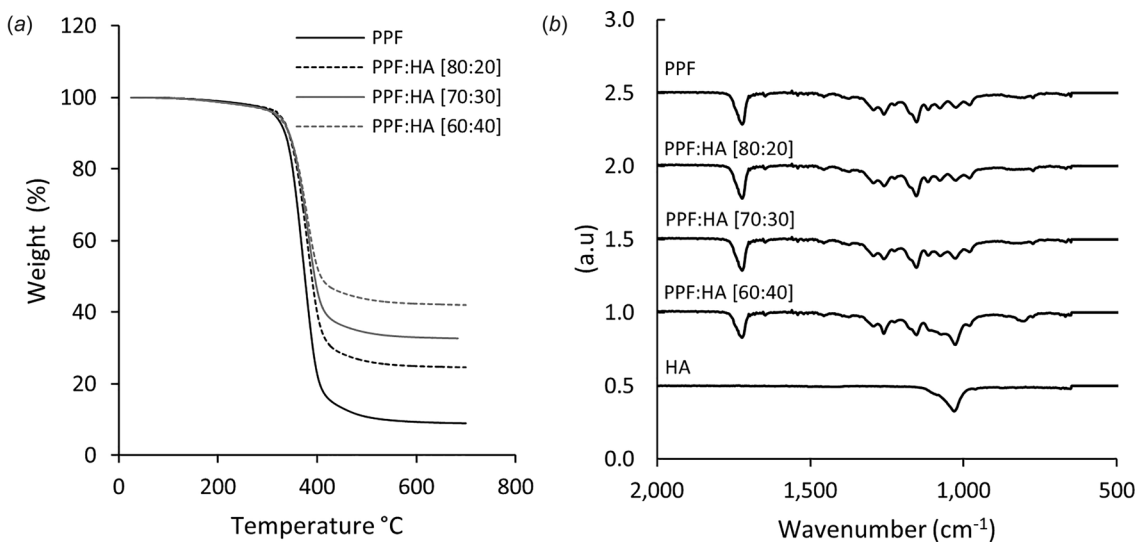

Fig. 3 (*a*) Thermal degradation and (*b*) FTIR spectra of the polymer groups

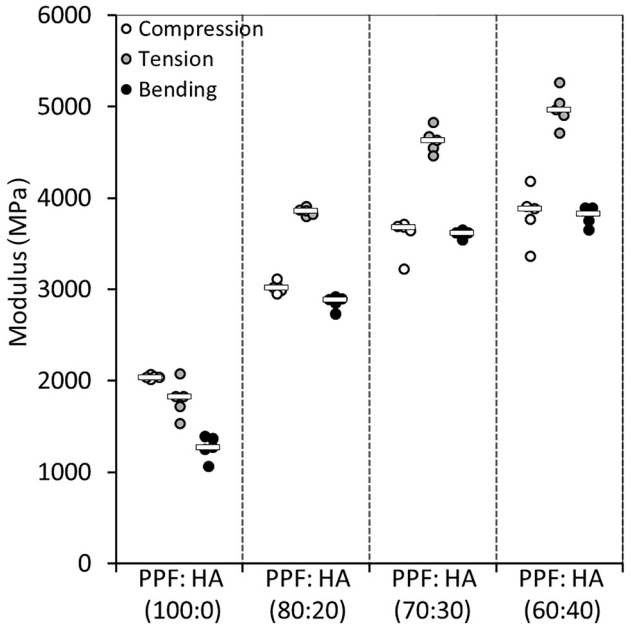

Fig. 4 Scatter plot showing the moduli outcomes of the polymer groups under compression, tension, and bending (bar represents the median)

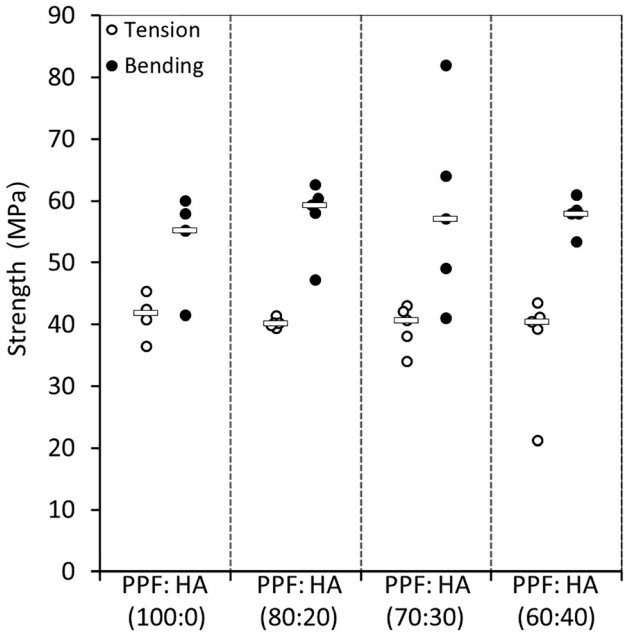

Fig. 5 Scatter plot showing the failure strength of the four material groups in tension and bending (bar represents the median)

moduli of the pure PPF in compression and tension were found to be about 2 GPa and 1.8 GPa, respectively. The mean chord modulus for bending was found to be about 1.3 GPa. The addition of HA significantly increased all moduli ($p < 0.0001$). The compressive modulus of PPF augmented with 20 wt % HA significantly increased by about 50%, and the tensile modulus increased by about twofold ($p < 0.0001$). This increase was larger in bending as the modulus changed from about 1.3 GPa to 2.9 GPa ($p < 0.0001$). With 30 wt % HA, all moduli continued to increase significantly ($p \leq 0.0008$), but the rate of increase became much lower when comparing that from pure PPF to PPF:HA (20 wt % HA). Except for the compressive modulus ($p = 0.23$), PPF:HA (40 wt % HA) showed significant increase in tensile and bending moduli compared with 30 wt % HA ($p \leq 0.0390$). The increase in tensile and bending moduli with the addition of 40 wt % HA, however, was only about 7.5% and 5.4% compared with 30 wt % HA.

Failure Strength. Fig. 5 shows the failure strength of the material formulations under tension and bending. Failure strength for pure PPF was about 41 MPa in tension and about 54 MPa in bending. Unlike the results observed for the moduli, the failure strength of PPF in tension and bending did not increase by HA augmentation ($p = 0.61$).

Hardness. Pure PPF showed a hardness of 65 M (Fig. 6). Hardness was improved significantly ($p < 0.0001$) by about 25% (81 M) when 20 wt % HA was added to pure PPF. Further addition of HA continued to improve the hardness outcomes ($p < 0.0001$), with PPF:HA (60:40) showing a hardness of about 90 M (~40% increase in hardness compared with pure PPF and ~10% when compared to 20 wt % HA).

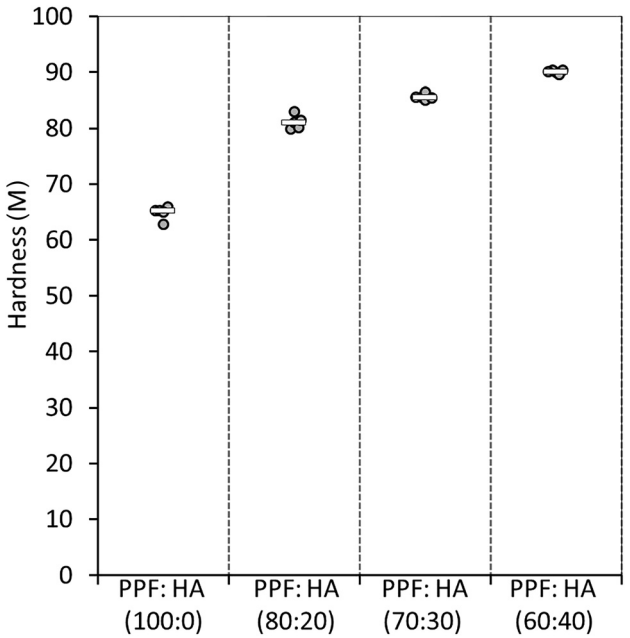

Fig. 6 Scatter plot showing the hardness outcomes for the four polymer groups (PPF; PPF:HA (80:20); PPF:HA (70:30); and PPF:HA (60:40)). The Rockwell hardness numbers (*M*) are based on an indenter size of 6.35 mm in diameter, a fixed small load of 10 kg, and a large load (100 kg). Bar represents the median.

Intervertebral Body Cages: Fabrication and Mechanical Testing. In total, 36 cages were fabricated and mechanically tested in compression. Figure 7 shows the mold designed and fabricated (Fig. 7(*a*)) to create the cages (Fig. 7(*b*)). Cages were fabricated using the polymer configurations previously described: PPF, PPF:HA (80:20), PPF:HA (70:30), and PPF:HA (60:40) (Fig. 7(*c*)). Figure 7(*d*) shows a pure PPF cage before compression testing, and Fig. 7(*e*) shows a porous PPF sample augmented with 40 wt % HA after compression testing.

Stiffness. To investigate the effect of HA, the cages with and without holes, as well as with porosity were combined and ANOVA was performed. The addition of HA increased the stiffness of all cages significantly ($p < 0.0001$). When considering all cages, augmentation of PPF with 20 wt % HA significantly increased the stiffness of pure PPF by about 84% ($p < 0.0001$; Fig. 8). The change in stiffness from 20 wt % HA to 30 wt % HA was only 12%, and from 30 wt % HA to 40 wt % HA only 6%. These changes were all insignificant ($p \geq 0.51$).

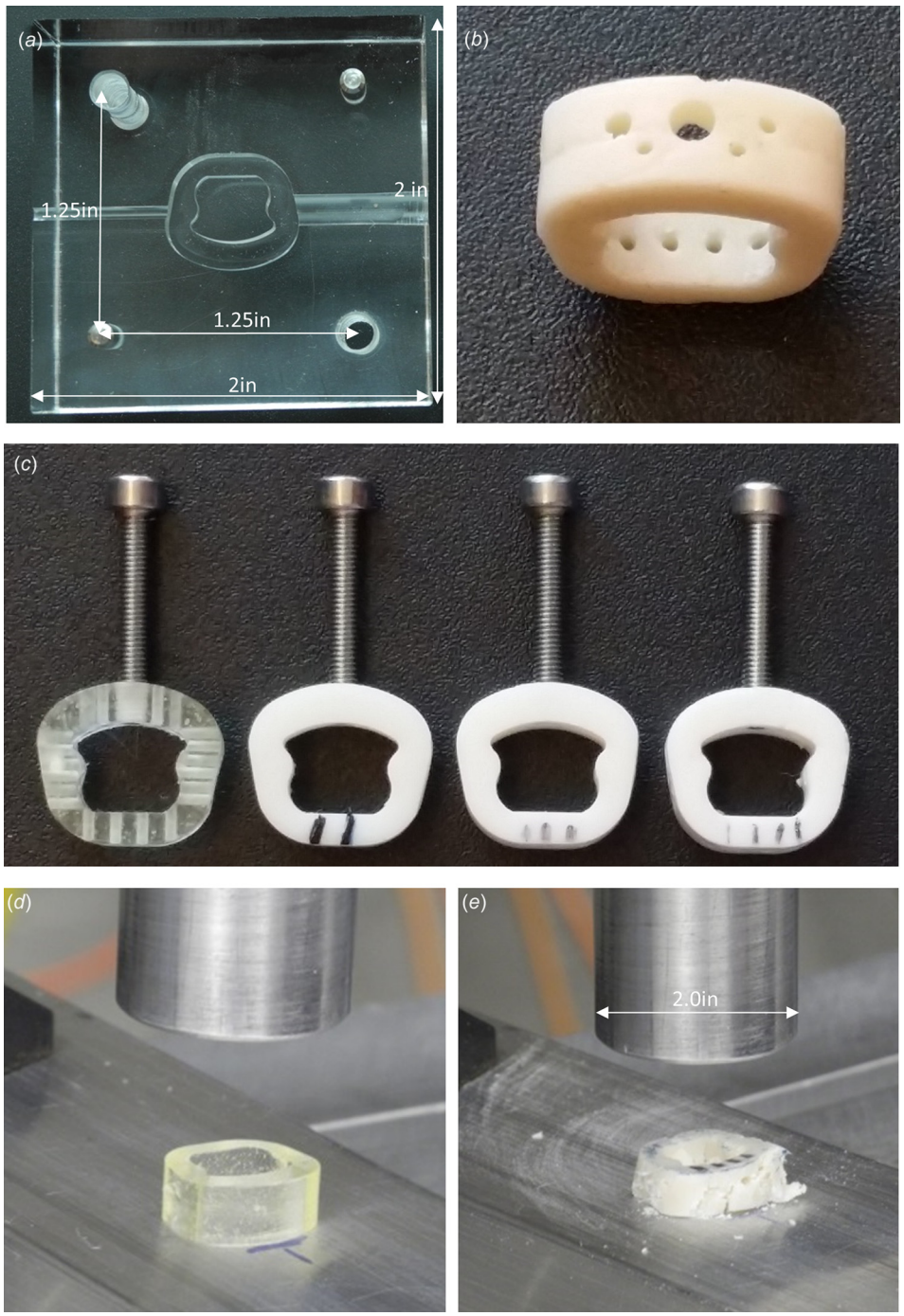

Fig. 7 Design, fabrication, and mechanical testing of cervical interbody fusion cages with and without porosity made of pure PPF and HA-augmented PPF: (*a*) a mold designed and fabricated to develop cages with no holes; (*b*) a fusion cage made out of 30 wt % HA-augmented PPF; (*c*) sample cages (PPF, left; 20, 30, and 40 wt% HA-PPF). Threaded holes and screws were also implemented to mimic the attachments used during a routine surgical technique. These threaded screws connect the cage with the holder used to place the cage in position between the vertebral bodies. The screws were removed during mechanical testing; (*d*) PPF cage before compression; and (*e*) porous PPF with 40 wt %HA after failure.

Analysis of variance was used to compare the cages without holes ($n = 12$), to cages with holes ($n = 12$), and the cages with holes and porosity ($n = 12$). The addition of holes did not significantly affect the stiffness of the cages ($p = 0.09$). The stiffness outcomes ranged from ~16,000 N/mm to about 35,000 N/mm for the cages without holes, depending on their HA augmentation. This trend was similar for the cages with holes, increasing in stiffness from about 11,500 N/mm to ~28,000 N/mm. Cages with holes and 50 wt % salt-induced porosity ranged in stiffness from about 11,000 N/mm to 24,000 N/mm. A significant difference was observed between cages with no holes and cages with holes and porosity ($p = 0.0073$). The cages with holes and porosity, on average, had lower stiffness than the cages with no holes by about 31%.

Failure Load. During compression testing of the nonporous cages with or without holes, a load of approximately 12 kN was

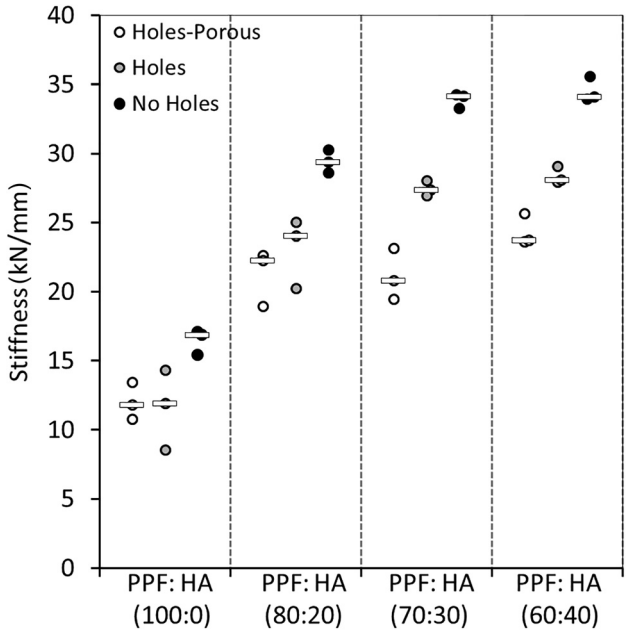

Fig. 8 Scatter plot showing the compressive stiffness outcomes for the cages: cages with no holes, cages with holes, and cages with holes and 50 wt % porosity (bar represents the median)

observed during testing, and the test was stopped to avoid damaging of the load cell. Interestingly, none of the nonporous cages (with or without holes) fractured during compression testing, regardless of the polymer group configuration, while porous cages fractured during compression testing (Fig. 7(*e*)). Compressive failure loads of porous cages varied from 2650 N for pure PPF to about 5000 N for PPF augmented with 20 wt % HA ($p = 0.0022$). Additional augmentation with HA (30 and 40 wt %) did not increase the failure load of the cages ($p \geq 0.49$).

Discussion

We have successfully augmented PPF with nano-HA, designed and fabricated intervertebral body cages, and showed the ability of HA-augmentation to affect the mechanical properties of these cages. ASTM-based mechanical testing on the bulk HA-augmented PPF showed that the addition of HA significantly increased the material properties of these nanocomposites. For pure PPF, the compressive modulus was found to be about 2 GPa, which increased to about 3 GPa with 20 wt % HA augmentation. Unlike porous cages, the nonporous cages, with and without holes, from the various polymer configurations, did not fail during compression testing.

Augmentation of PPF by 20 wt % HA significantly increased the moduli (compression, bending, and tension) of pure PPF. However, although still increasing, the increment between 30 wt % and 40 wt % HA PPF-augmentation was not as significant as that observed between pure PPF and 20 wt % HA augmented PPF. These outcomes were consistent with those observed during the compression testing of the cages. Augmentation of the cages with more than 20 wt % HA did not significantly improve their compressive stiffness. A possible reason for these outcomes could be incomplete or poor photo crosslinking of the polymer with higher ratios of HA. The addition of artificial holes with 50 wt % salt-induced porosity did not significantly reduce structural properties of the cages. This is important as holes or porosity could potentially be used to enhance bone ingrowth without compromising the structural integrity of the cages.

Titanium cages combined with bone grafts can result in proper fusion. However, there may be several postoperative complications such as stress shielding due to the cages having a much higher elastic modulus than bone, cage migration, and cage subsidence [5,15]. On the other hand, although PEEK cages have a similar elastic modulus to cortical bone, reducing the effect of stress shielding [16], these cages are not biodegradable, and more importantly, they show poor osseointegration with the surrounding tissue. These shortcomings cause micromotion and possible nonunions of the bony structures, eventually preventing long-term stability of the spine [16,17]. PPF:HA biocomposite materials are biodegradable and can provide similar mechanical properties as those from bone. Further implementation of salt can also allow for porosity in the structure to help and enhance osseointegration of the cage-bone system. Interestingly, a PPF-based composite material was shown to increase its mechanical properties over a course of 12 weeks of in vitro degradation [9,18]. A 12-week period could allow for bone formation in those areas while still maintaining enough mechanical support.

Due to its biocompatibility, biodegradability, cross-linking properties, and osteoconductivity, PPF has been proposed for numerous orthopedic and dental applications [19]. PPF, with similar mechanical properties as cancellous bone [9], has been considered a good candidate for injectable orthopedic implants and the repair of bone defects [20]. Interestingly, previous studies have shown PPF augmented with HA to achieve improved biocompatibility. Lewandrowski et al. [21] found enhanced osteoconductive properties of PPF with HA, leading to accelerated bone formation around and within the scaffold. Lee et al. [22] showed better cell adhesion and proliferation when PPF:DEF augmented with HA was used compared with PPF:DEF scaffolds alone. Improved material properties of PFF with various concentrations of HA were observed in this study. Additionally, we showed a different application of these materials for cervical spine fusion treatment. Augmenting PPF with HA not only enhances the biocompatibility and bioactivity of PPF [21,22], but it enhances its structural integrity potentially making it a suitable candidate for intervertebral body fusion.

In this study, the nonporous cages from all polymer configurations reached high load limits during testing without failing or breaking (about 12 kN). On the other hand, the failure load (larger than 5000 N) of the 20 wt % HA augmented-PPF porous cages with holes found in our study was considerably larger than the previously reported average failure loads of cervical vertebral bodies (2400–3400 N) [23,24]. This suggests that the PPF porous cages with 20 wt % HA and holes can provide good structural integrity to the spine segment. Furthermore, by adding about 50 wt % porosity to the construct, in addition to attaining the desire mechanical stability, osseointeration and faster bone tissue ingrowth could be guaranteed.

This study has several limitations. First, although a higher amount of salt incorporation would result in higher porosity and more space for bone ingrowth, at above 50 wt %, our PPF:HA–salt mixture became very viscous, preventing adequate stirring/mixing for homogenous crosslinking. For this reason, up-to 50 wt % of salt particles was used in this study. Second, while we intended to create a porosity of 50 wt % by adding and then leaching out NaCl, similar to previous studies [20], we did not investigate whether there were some remnants of salt within the cages. Remaining salt within the cages might have affected the mechanical outcomes of the cages. Additionally, nonuniform incorporation of HA and salt may have induced unintentionally anisotropic behavior of the material, affecting the final mechanical properties. Future studies should perform imaging, such as microcomputed tomography to visualize and evaluate porosity within the structure. Third, we did not perform a power analysis, and the sample size from the cages with various polymer configurations was small for statistical analyses. However, the quantitative outcomes from the groups are large to ensure potential differences between the groups. Fourth, although intended to potentially facilitate vascularization, nutrients and waste transport, hole location will affect mechanical properties of the cages. A future study should evaluate

various locations, sizes, and number of holes to allow for an optimum outcome. Finally, while out of the scope of this paper, we acknowledge that micromotion and subsidence are important aspects to consider in the development of intervertebral body cages.

In this study, an increase in the elastic moduli, from about 2 GPa to 5 GPa, was obtained by incorporating HA into the PPF formulation. While these values fall within the wide range of outcomes (350–20 GPa) [25–27] obtained for trabecular bone, these are lower than those obtained for cortical bone. However, intervertebral body cages developed using PPF augmented with HA showed large compressive properties suitable for providing the necessary load bearing capacity and potential stability to the spine. A future cadaveric study would provide additional information regarding variability in surgical techniques, surgeon variability, subsidence, and micromotion of these cages.

In conclusion, PPF augmented with HA can be a suitable material of choice for cages to be used in cervical intervertebral body fusion. A complete mechanical characterization has been performed of PPF augmented with HA. The addition of 20 wt % HA to PPF was sufficient to significantly enhance the material and structural properties of the cages, with additional HA augmentation having a minimal effect. Due to the structural performance of PPF augmented with HA, holes and/or porosity can be added to the intervertebral cages to promote bone ingrowth without significantly compromising its structural integrity.

Acknowledgment

The content is solely the responsibility of the authors and does not necessarily represent the official views of the National Institutes of Health.

Funding Data

- National Institute of Arthritis and Musculoskeletal and Skin Diseases of the National Institutes of Health (R01 AR56212).
- National Institute of Biomedical Imaging and Bioengineering of the National Institutes of Health (F32EB023723).
- National Natural Science Foundation of China (31360229).

References

[1] Navarro, M., Michiardi, A., Castano, O., and Planell, J., 2008, "Biomaterials in Orthopaedics," J. R. Soc. Interface, **5**(27), pp. 1137–1158.

[2] Geetha, M., Singh, A., Asokamani, R., and Gogia, A., 2009, "Ti Based Biomaterials, the Ultimate Choice for Orthopaedic Implants—A Review," Prog. Mater. Sci., **54**(3), pp. 397–425.

[3] Hojo, Y., Kotani, Y., Ito, M., Abumi, K., Kadosawa, T., Shikinami, Y., and Minami, A., 2005, "A Biomechanical and Histological Evaluation of a Bioresorbable Lumbar Interbody Fusion Cage," Biomaterials, **26**(15), pp. 2643–2651.

[4] Martz, E. O., Goel, V. K., Pope, M. H., and Park, J. B., 1997, "Materials and Design of Spinal Implants—A Review," J. Biomed. Mater. Res. Part A, **38**(3), pp. 267–288.

[5] van Dijk, M., Smit, T. H., Sugihara, S., Burger, E. H., and Wuisman, P. I., 2002, "The Effect of Cage Stiffness on the Rate of Lumbar Interbody Fusion: An In Vivo Model Using Poly (l-Lactic Acid) and Titanium Cages," Spine, **27**(7), pp. 682–688.

[6] McAfee, P. C., Cunningham, B. W., Lee, G. A., Orbegoso, C. M., Haggerty, C. J., Fedder, I. L., and Griffith, S. L., 1999, "Revision Strategies for Salvaging or Improving Failed Cylindrical Cages," Spine, **24**(20), pp. 2147–2153.

[7] Tullberg, T., 1998, "Failure of a Carbon Fiber Implant: A Case Report," Spine, **23**(16), pp. 1804–1806.

[8] He, S., Timmer, M., Yaszemski, M. J., Yasko, A., Engel, P., and Mikos, A., 2001, "Synthesis of Biodegradable Poly (Propylene Fumarate) Networks With Poly (Propylene Fumarate)-Diacrylate Macromers as Crosslinking Agents and Characterization of Their Degradation Products," Polymer, **42**(3), pp. 1251–1260.

[9] Yaszemski, M. J., Payne, R. G., Hayes, W. C., Langer, R., and Mikos, A. G., 1996, "In Vitro Degradation of a Poly (Propylene Fumarate)-Based Composite Material," Biomaterials, **17**(22), pp. 2127–2130.

[10] Wei, G., and Ma, P. X., 2004, "Structure and Properties of Nano-Hydroxyapatite/Polymer Composite Scaffolds for Bone Tissue Engineering," Biomaterials, **25**(19), pp. 4749–4757.

[11] Woodard, J. R., Hilldore, A. J., Lan, S. K., Park, C., Morgan, A. W., Eurell, J. A. C., Clark, S. G., Wheeler, M. B., Jamison, R. D., and Johnson, A. J. W., 2007, "The Mechanical Properties and Osteoconductivity of Hydroxyapatite Bone Scaffolds With Multi-Scale Porosity," Biomaterials, **28**(1), pp. 45–54.

[12] Wang, S., Lu, L., Gruetzmacher, J. A., Currier, B. L., and Yaszemski, M. J., 2005, "A Biodegradable and Cross-Linkable Multiblock Copolymer Consisting of Poly (Propylene Fumarate) and Poly (ε-Caprolactone): Synthesis, Characterization, and Physical Properties," Macromolecules, **38**(17), pp. 7358–7370.

[13] Fisher, J. P., Dean, D., and Mikos, A. G., 2002, "Photocrosslinking Characteristics and Mechanical Properties of Diethyl Fumarate/Poly (Propylene Fumarate) Biomaterials," Biomaterials, **23**(22), pp. 4333–4343.

[14] Weissgerber, T. L., Milic, N. M., Winham, S. J., and Garovic, V. D., 2015, "Beyond Bar and Line Graphs: Time for a New Data Presentation Paradigm," PLoS Biol, **13**(4), p. e1002128.

[15] Kanayama, M., Cunningham, B. W., Haggerty, C. J., Abumi, K., Kaneda, K., and McAfee, P. C., 2000, "In Vitro Biomechanical Investigation of the Stability and Stress-Shielding Effect of Lumbar Interbody Fusion Devices," J. Neurosurg.: Spine, **93**(2), pp. 259–265.

[16] Kurtz, S. M., and Devine, J. N., 2007, "PEEK Biomaterials in Trauma, Orthopedic, and Spinal Implants," Biomaterials, **28**(32), pp. 4845–4869.

[17] Olivares-Navarrete, R., Gittens, R. A., Schneider, J. M., Hyzy, S. L., Haithcock, D. A., Ullrich, P. F., Schwartz, Z., and Boyan, B. D., 2012, "Osteoblasts Exhibit a More Differentiated Phenotype and Increased Bone Morphogenetic Protein Production on Titanium Alloy Substrates Than on Poly-Ether-Ether-Ketone," Spine J., **12**(3), pp. 265–272.

[18] Timmer, M. D., Ambrose, C. G., and Mikos, A. G., 2003, "In Vitro Degradation of Polymeric Networks of Poly(Propylene Fumarate) and the Crosslinking Macromer Poly(Propylene Fumarate)-Diacrylate," Biomaterials, **24**(4), pp. 571–577.

[19] Hollinger, J. O., 2011, *An Introduction to Biomaterials*, 2nd ed., CRC Press, Boca Raton, FL.

[20] Fisher, J. P., Vehof, J. W., Dean, D., van der Waerden, J. P., Holland, T. A., Mikos, A. G., and Jansen, J. A., 2002, "Soft and Hard Tissue Response to Photocrosslinked Poly (Propylene Fumarate) Scaffolds in a Rabbit Model," J. Biomed. Mater. Res. Part A, **59**(3), pp. 547–556.

[21] Lewandrowski, K. U., Bondre, S. P., Wise, D. L., and Trantolo, D. J., 2003, "Enhanced Bioactivity of a Poly (Propylene Fumarate) Bone Graft Substitute by Augmentation With Nano-Hydroxyapatite," Bio-Med. Mater. Eng., **13**(2), pp. 115–124.

[22] Lee, J. W., Ahn, G., Kim, D. S., and Cho, D.-W., 2009, "Development of Nano-and Microscale Composite 3D Scaffolds Using PPF/DEF-HA and Micro-Stereolithography," Microelectron. Eng., **86**(4–6), pp. 1465–1467.

[23] Przybyla, A. S., Skrzypiec, D., Pollintine, P., Dolan, P., and Adams, M. A., 2007, "Strength of the Cervical Spine in Compression and Bending," Spine (Phila Pa 1976), **32**(15), pp. 1612–1620.

[24] White, A. A., and Panjabi, M. M., 1990, *Clinical Biomechanics of the Spine*, Lippincott, Philadelphia, PA.

[25] Brennan, O., Kennedy, O. D., Lee, T. C., Rackard, S. M., and O'Brien, F. J., 2009, "Biomechanical Properties Across Trabeculae From the Proximal Femur of Normal and Ovariectomised Sheep," J. Biomech., **42**(4), pp. 498–503.

[26] Giambini, H., Wang, H. J., Zhao, C., Chen, Q., Nassr, A., and An, K. N., 2013, "Anterior and Posterior Variations in Mechanical Properties of Human Vertebrae Measured by Nanoindentation," J. Biomech., **46**(3), pp. 456–461.

[27] Lai, Y. S., Chen, W. C., Huang, C. H., Cheng, C. K., Chan, K. K., and Chang, T. K., 2015, "The Effect of Graft Strength on Knee Laxity and Graft In-Situ Forces After Posterior Cruciate Ligament Reconstruction," PLoS One, **10**(5), p. e0127293.